Physica B 405 (2010) 4517–4522

Contents lists available at ScienceDirect

Physica B

journal homepage: www.elsevier.com/locate/physb

# Single layer porous gold films grown at different temperatures

Renyun Zhang*, Magnus Hummelgård, Håkan Olin

*Department of Natural Sciences, Engineering and Mathematics, Mid Sweden University, SE-851 70 Sundsvall, Sweden*

ARTICLE INFO

*Article history:*
Received 9 June 2010
Received in revised form
4 August 2010
Accepted 6 August 2010

*Keywords:*
Gold film
Porous
Single layer
Temperature
Coalescence

ABSTRACT

Large area porous gold films can be used in several areas including electrochemical electrodes, as an essential component in sensors, or as a conducting material in electronics. Here, we report on evaporation induced crystal growth of large area porous gold films at 20, 40 and 60 °C. The gold films were grown on liquid surface at 20 °C, while the films were grown on the wall of beakers when temperature increased to 40 and 60 °C. The porous gold films consisted of a dense network of gold nanowires as characterized by TEM and SEM. TEM diffraction results indicated that higher temperature formed larger crystallites of gold wires. An in situ TEM imaging of the coalescence of gold nanoparticles mimicked the process of the growth of these porous films, and a plotting of the coalescence time and the neck radius showed a diffusion process. The densities of these gold films were also characterized by transmittance, and the results showed film grown at 20 °C had the highest density, while the film grown at 60 °C had the lowest consistent with SEM and TEM characterization. Electrical measurements of these gold films showed that the most conductive films were the ones grown at 40 °C. The conductivities of the gold films were related to the amount of contamination, density and the diameter of the gold nanowires in the films. In addition, a gold film/gold nanoparticle hybrid was made, which showed a 10% decrease in transmittance during hybridization, pointing to applications as chemical and biological sensors.



## 1. Introduction

Thin metal films with or without porous structures have unique properties that are different from bulk materials. These films have many different nanoscale morphologies such as island films, hillocks films and holey films [1]. The optical and electronic behavior of thin metal films is associated with the film morphology [2], for example, thin gold films have excellent tailorable surface plasmon resonances, surface enhanced Raman scattering and highly enhanced fluorescence properties, which allows ultrahigh sensitivity down to single molecule level due to this dramatic enhancement [3,4].

To fabricate thin porous films, methods like dealloying [5–8], templating [9–11], wet chemical [12,13], electrochemical deposition [14] and evaporation induced self-assembly are used [15–17]. Among these methods, evaporation induced film growth from nanoparticles are of interest due to its simple method. Generally, the nanoparticles are self-assembled and form ordered 3D structures [18–21]. But, for gold nanoparticles, the self-assembled nanoparticles could form disordered networks of nanowires with [16] or without [17] surfactants at room temperature.

We reported earlier about the fabrication of porous gold films using evaporation induced crystal growth at room temperature [17]. However, the growth mechanism is not clear, in particular the temperature dependency needs to be investigated, since it is an important parameter during evaporation induced growth of films. A coalescence process of the gold nanoparticles [22] was discussed in Ref. [17] as an essential part of the growth mechanism, but more work is needed to show or mimic the process.

Here, we describe a study of single layer porous gold films at different growth temperature, as well as their optical and electrical properties. Moreover, the crystal growth of gold nanoparticles was investigated in situ by TEM, which showed the coalescence of gold nanoparticles. Transmittance measurements indicated that the evaporation speed at different temperature caused the different film density, and the electrical measurements showed that the conductivity of the gold film was due to contamination in the film, the film density and the diameter of the gold wires in the film. Moreover, a gold film/gold nanoparticle hybrid was fabricated using hexamethylene diamine (HD) as a linking molecule, suggesting potential application of these gold films as sensors.

## 2. Experimental

### 2.1. Synthesis of gold nanoparticles

1.0 ml 1.0 wt% $HAuCl_4$ (Sigma) solution was added into 99.0 ml doubly distilled water and heated to boil while stirring, then,

* Corresponding author. Tel.: +46 60 148484; fax: +46 60 148802.
*E-mail address:* renyun.zhang@miun.se (R.Y. Zhang).

0921-4526/$ - see front matter © 2010 Elsevier B.V. All rights reserved.
doi:10.1016/j.physb.2010.08.029

4.0 ml 1.0 wt% sodium citrate (Sigma) was added [23]. The solution was kept boiling for 5 to 10 min, until the solution turned to a red wine color.

### 2.2. Self-assembly of gold film

The synthesized colloid gold solution was stored in 100 ml beakers with an internal diameter of 6 cm, separately. The beakers were then covered by a 1000 ml beaker in order to avoid dust from air. To grow gold films, the beakers were stored at $20 \pm 2$, $40 \pm 1$ and $60 \pm 1$ °C, separately, with humidity of about $30 \pm 2\%$. At the temperature of 60 °C, a single layer porous gold film was found on the beaker wall after one days growth, while it took 2 to 4 days for the temperature of 40 °C. The film that grown at 20 °C was found floating on the solution surface, after 4 to 7 days growth.

### 2.3. Fabrication of gold film/gold nanoparticle hybrid

The gold film was subtracted by a glass slide, and rinsed with doubly distilled water for 5 min by re-floating the film on the water surface. Then the film was subtracted again and floats on the solution that contains 10.0 wt% hexamethylene diamine (HD) for 10 min to let the modification of HD on gold wires. After that the film was subtracted again and rinsed by doubly distilled water for 10 min to remove the physically absorbed HD. Subsequently, we subtracted the film and float it on gold nanoparticle solution that was prepared as above. The hybrid time was also 10 min. At last the gold film was subtracted and rinsed by doubly distilled water as described above for further measurements.

### 2.4. TEM and SEM characterizations

For TEM characterization, 400 Mesh gold grid without carbon film was put under the floating gold film, and by retracting the film was deposited on the grid. The grid was dried at room temperature for 20 min. TEM imaging was done using a JEOL 2000FX transmission electron microscope at 160 kV accelerate voltage. To investigate the crystal growth of gold nanoparticles, the electron beam was focused on two neighbor gold nanoparticles for 30 min at beam current densities of 250 to 320 pA/cm$^2$. SEM and SEM-EDX characterizations were performed on an EVO50 (Zeiss). The samples for SEM were prepared by coating the gold film on a SiO2 wafer.

### 2.5. Transmittance and electric measurements

Transmittance measurements of gold films were done using an Edmund CCD spectrometer. The films were deposited on standard glass slides that were rinsed with acetone, $H_2SO_4/HNO_3$ (v/v, 3:1) and doubly distilled water.

I/V measurements were performed on a micromanipulator 1800 wafer probe station (Micromanipulator), using two stainless wires as source and drain electrodes. Sheet resistance measurements were done using a Magne-Tron M800A four-point probe system.

## 3. Results and discussion

In an earlier report [17], we found that the gold film floated on surface of the solution with an area up to several square centimeters at about 21 °C. This floating film was usually deposited on a substrate by a simple subtracting procedure. For example, a glass slide was dipped into the solution and a floating film was then picked up by retracting the slide.

However, when the evaporation temperature increased to 40 and 60 °C, no such floating film was present, instead the films were deposited on the walls of the beakers. To deposit these films on a substrate, we added more water and the films on the beaker walls detached and floated on the solution surface. Then these films were deposited by the same simple subtracting procedure.

The reason for this non-floating behavior at higher temperature might be related to the corresponding higher evaporation rate of the solution and interplay with surface energies. At 21 °C, the evaporation speed was slow and the coalescence of gold nanoparticles was extended to the solution surface. While at higher temperatures and higher evaporation speeds, the crystal coalescence of gold nanoparticles could just occur on the wall.

Fig. 1 shows the TEM images of the single layer gold films that were obtained at different temperature. The average diameter of gold wires in the films were 100, 70 and 75 nm for the growing temperature of 20, 40 and 60 °C, respectively. The procedure to calculate the average diameter was by taking 10 random places in each image and averaging them.

The widest gold wires were observed at 20 °C. However, the nanowires on the films that were grown at 60 °C were a few nanometer wider than those grown at 40 °C, despite the higher evaporation speed at 60 °C. TEM diffraction pattern also indicated that a higher temperature caused larger crystallites (see supplementary materials). We note that the 20 °C films were of the floating type, and as they were surrounded by gold nanoparticles for a longer time than in those films that were grown on the wall of beakers, it is not so surprising that they have wider nanowires. The slight increase in the diameter of the nanowires at 60 °C compared to 40 °C might be due to increased diffusion rate in the solution or increased rate of coalescence (see discussion below). We should also note that the TEM images show floating films that were picked up from the solution and rinsed with water, and in the case of growing on the beaker walls, any minor particles, between the network, sticking to the surface should remain there and will not appear in the TEM images.

The EISA method is usually used for growing crystals of some hundred nm large spheres, usually glass, for applications such as photonic lattices. This EISA growth is layer-by-layer, or Stranski–Kastanov (SK) growth forming an almost perfect crystal of spheres.

In the present study, the growth is very different from this SK growth; instead we have the Volmer–Weber mode of growth, also called island growth, which formed porous single layers with gold nanowire networks. Such island growth is present when the particles stick where they land and have low mobility on the surface [24]. The network in our experiment is then the result of growing islands that touch each other and coalesce [25]. In our case we have three important processes: (1) the diffusion of gold nanoparticles in the solution, (2) the sticking events when the particles land on the beaker wall or on already assembled gold-islands and (3) the coalescence of particles and islands.

The gold nanoparticles in solution diffuse due to Brownian motion. The particles diffuse to the capillary interface and adsorb at the beaker wall or to the gold network. This Brownian motion is depended on the temperature of the solution. The adsorbed gold nanoparticles can form aggregates during their sticking on beaker wall, and subsequently coalesced into some islands, and later form networks. There are several models for similar kind of growth. The aggregation of gold clusters to form island has been investigated by Werner et al. [26] showing the diffusion and fusion of small gold clusters (50 to 300 atoms). Jensen and coworkers develop a deposition, diffusion and aggregation (DDA) model [27] to simulate the growth of thin porous film, generating

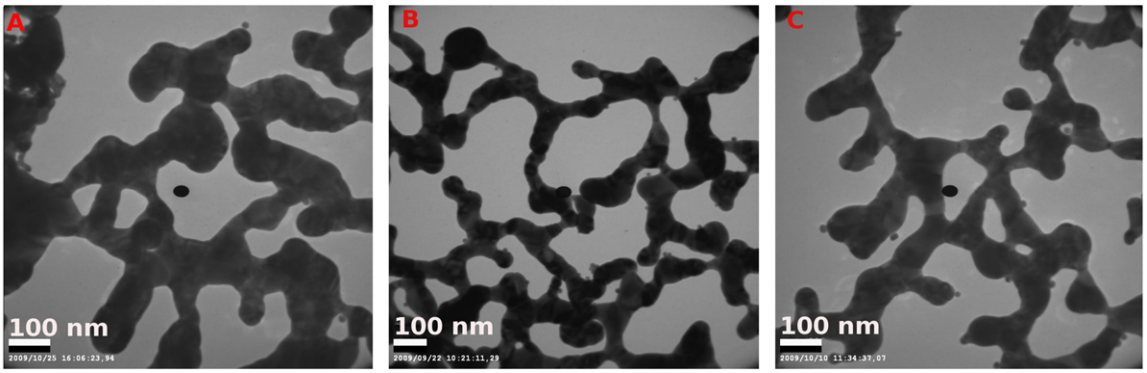


**Fig. 1.** TEM images of single layer gold films that were fabricated at about 20 (A), 40 (B) and 60 °C (C). The black dots in the center are the imaging artifacts.

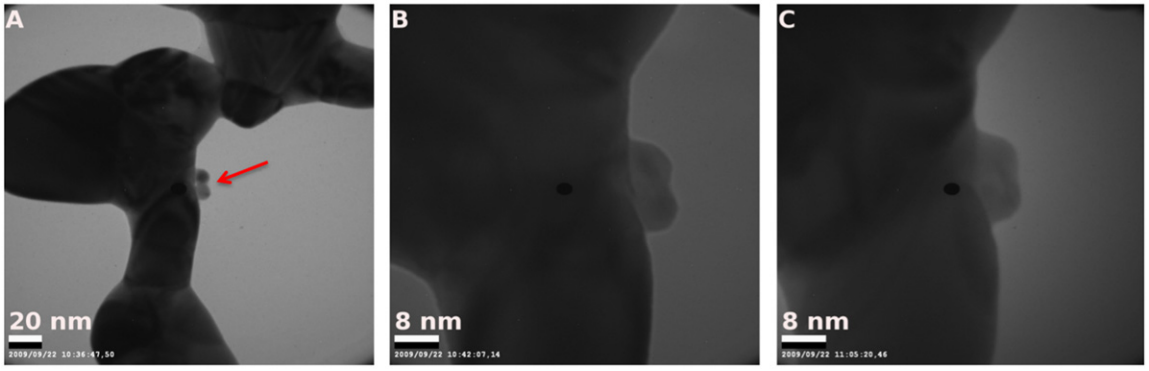


**Fig. 2.** In situ imaging of the coalescence process of gold nanoparticles under electron beam irradiation inside a TEM. Images show the initial status of two neighboring gold nanoparticles (A). After 6 (B), and 30 min (C) of electron beam irradiation. The black dot in the center is an imaging artifact.

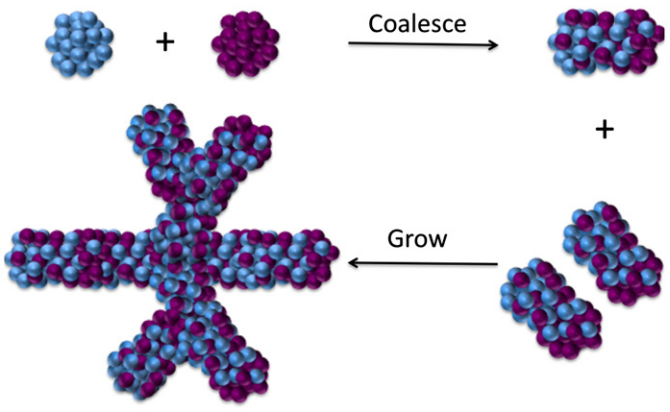


**Fig. 3.** Schematic draw of the coalescence of two gold nanoparticles and the growth of gold nanowire network.

fractal structures characteristic of diffusion limited aggregation (DLA) [28] and cluster–cluster aggregation (CCA) [29]. Here, we lack the details for any such quantitative modeling, but we note that the DDA model might fit well, as all relevant processes are included.

The coalescence process is the basic process for fusing two or more gold nanoparticles into larger islands. It began with the contact of two gold nanoparticles, and might be followed by the orientational alignment of coalescing planes at the contacted interface [30,31].

The main driving force for the coalescence is the reduction in surface energy when the area is reduced. When two particles meet, the gold atoms diffuse on the surface until the combined surface area, and thus the surface energy, is minimized. In the case of two particles this is when the particles coalescence into a single one, while, on a larger surface the small particles will coalescence into the larger structure and disappear.

Since the coalescence of gold nanoparticles in the growth of films occurred on a liquid surface or on the wall of a beaker, it was hard to directly observe the growth process. However, to get some more information about the growth process, we studied one of the growth steps, the coalescence of the gold nanoparticles, using in situ TEM. We focused the electron beam, which is known to induce coalescence of gold nanoparticles [22], on two neighboring gold nanoparticles that were absorbed on a gold nanowire.

Fig. 2 shows the in situ TEM images of the gold coalescence under electron beam radiation. In the beginning, the two gold nanoparticles were connected, but clearly as two separated nanoparticles. However, when these two gold nanoparticles were under electron irradiation for 6 min, it was found that the two nanoparticles coalesced and became one particle. After 30 min irradiation, these two gold nanoparticles were totally coalesced into a single particle. In the real solution growth process, more nanoparticles were present in the vicinity and causing further growth and extension of length and width. Fig. 3 illustrates schematically the coalescence of two gold nanoparticles. Two neighboring gold nanoparticles adsorbed and connected, exchange atoms with each other and the two particles coalesce into a single particle. By repeating this process, more and more gold nanoparticles coalesced and formed gold nanowire networks (see Fig. 3). Experimentally, we found similar coalescence process, as shown in Fig. 4. It is clear that there are three big parts that were connected with several small gold nanoparticles. Fig. 4(B–D) clearly shows that the small gold nanoparticles coalesced with time and the three big parts have been grown into one single gold wire. These observations make the process illustrated in Fig. 3 likely.

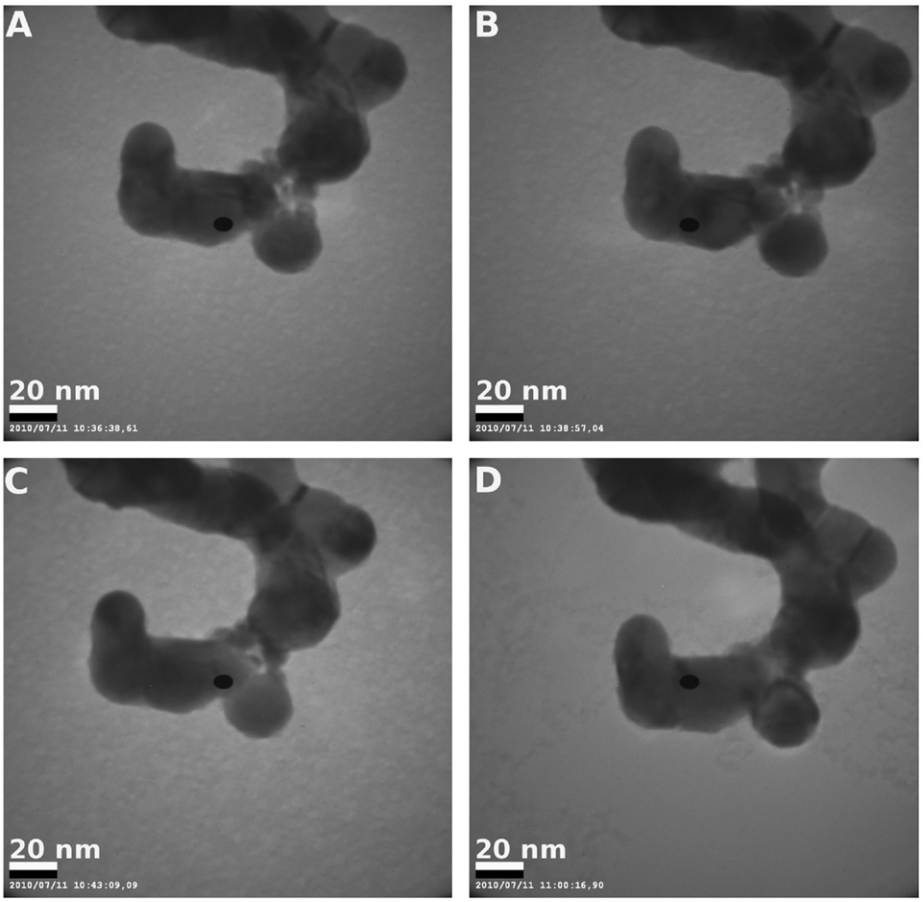


**Fig. 4.** TEM images of the coalescence of gold nanoparticles into gold wire, (A) the beginning of the coalescence, and (B) after 2, (C) 5 (D) and 24 min of coalescence.

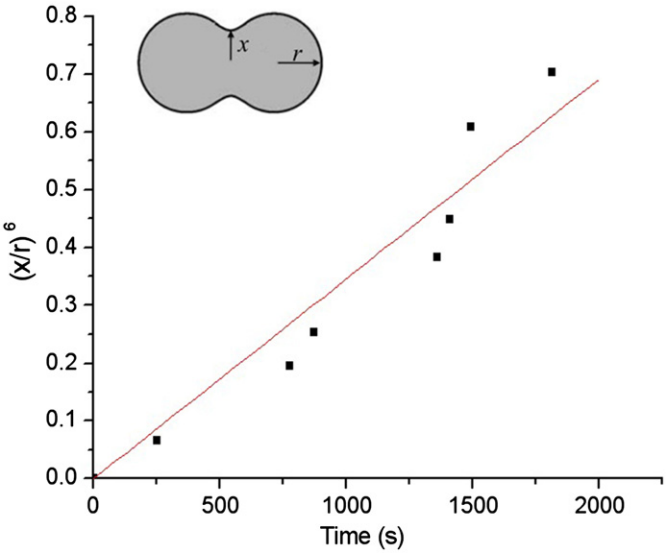


**Fig. 5.** Plot of the coalescence time versus $(x/r)^6$.

There are different mechanisms for the coalescence of two solid nanoparticles. For particles with a radius lager than 2 nm, surface diffusion or grain boundary diffusion are dominant, which can be expressed [32,33] as

$$t = \frac{(x/r)^6 r^4 RT}{CwD\sigma_{sv}\Omega} \quad (1)$$

where $t$ is the coalescence time, $x$ the neck radius, $r$ the initial particle radius, $R$ the gas constant, $T$ the temperature, $C$ a constant, $\Omega$ the molar volume, $w$ the surface or grain boundary layer width (estimated from $\Omega^{1/3}$) and $\sigma_{sv}$ the solid–vapor surface tension. In Fig. 5 the coalescence time and $(x/r)^6$ are plotted, and a fit indicates a linear relationship between these two parameters. Using Eq. (1), we found the calculated value of $C$ to be about $1.7 \times 10^{-15}$ from the slope.

Fig. 6 shows SEM images of gold films that were fabricated at different temperature. The density of gold nanowires was highest at the growing temperature of 20 °C. The density of gold nanowires for the film grown at 40 °C seemed to be higher than the one grown at 60 °C, but it was not easy to quantify this from the SEM images. However, transmittance measurements of these gold films showed larger differences. Fig. 7 shows the transmittance curves of these three kinds of gold films at wavelengths between 400 and 800 nm. The film grown at 20 °C has the lowest transmittance, and the film grown at 40 °C was lower than that of 60 °C. As mentioned above in the TEM imaging, the wire diameter of 60 °C films was larger that of the 40 °C ones. However, in the optical measurements, the transmittance of the 60 °C film was higher than for the 40 °C film, indicating that the 60 °C film had a lower density than that of the 40 °C film. This may be because the evaporation speed of water for 60 °C was higher than that of 40 °C. Moreover, the water flux inside the solution was also higher at 60 °C, which could also be a factor influencing the film density.

The electrical properties of these gold films were also investigated. The sheet resistance of the films was measured by four points measurements, and at 20, 40 and 60 °C the sheet resistance ($R_s$) was 120, 25 and 28 Ω/sq, respectively. Current–voltage (I/V) curves these gold films are shown in Fig. 8. The

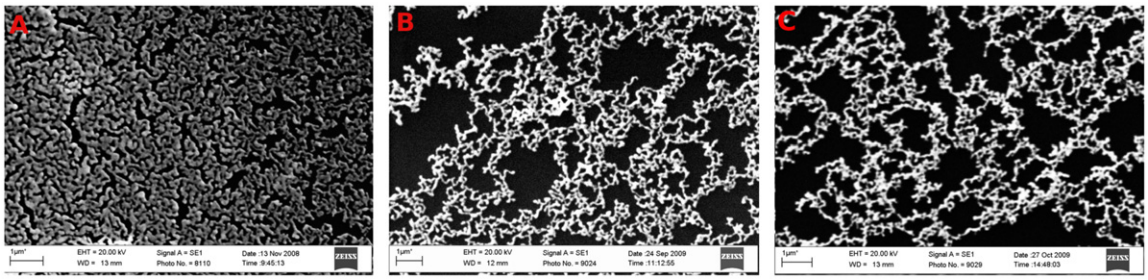


**Fig. 6.** SEM images of gold films grown at 20, 40 and 60 °C. Scale bar:1 μm.

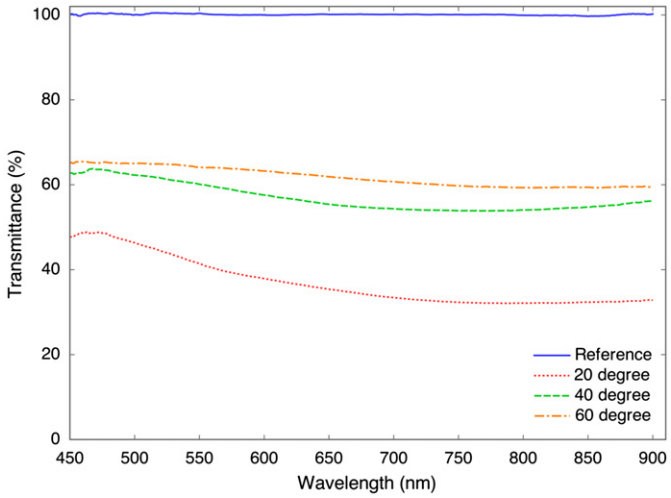


**Fig. 7.** Transmittance of gold films grown at different temperature.

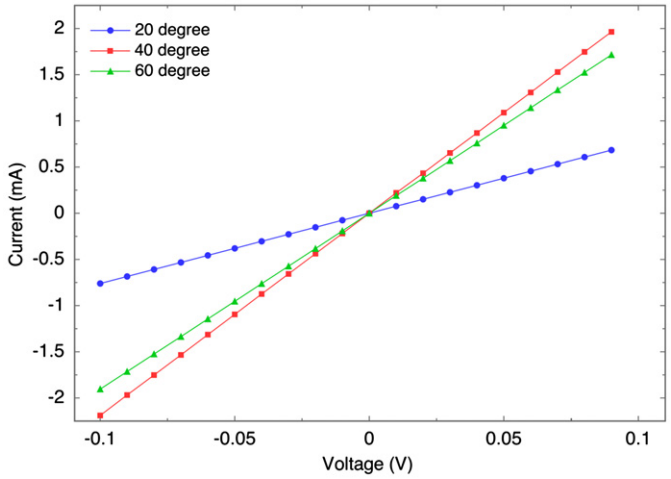


**Fig. 8.** I/V measurements of the gold films grown at different temperature.

resistances for these three gold films were about 135, 45 and 55 Ω. Sheet resistance and I/V measurements indicated that the film grown at 40 °C has the highest conductivity, while the film grown at 20 °C has the lowest. These results could be compared with a perfect 100 nm thick gold film with bulk resistivity that should have a sheet resistance of 0.2 Ω/sq (from $R_s$ = resistivity/thickness and bulk resistivity of 22 nΩ/m), or a deposited gold film with 42 nm thickness that has a $R_s$ of 1.5 Ω/sq [34], or with porous gold film fabricated on a porous aluminum template that has a 2 of 4–15 Ω/sq for a film thickness of about 100 nm [35].

If the film grown at 20 °C had the largest nanowire width and highest density, it should have the highest conductivity, but it was found to have the lowest. The reason for this could be a result of contamination of the gold films. The film grown at 20 °C was floating on the surface of the solution, and sodium citrate molecules, which still should be in the solution, might contribute to contamination of the gold films, causing an increase in resistance. For the floating film this exposure to a contaminating solution lasts for the entire growth process. In contrast, when the films were deposited on the beaker walls, as in the high temperature cases, the exposure to a contaminating solution is only for a shorter timespan. Fig. S2 in supporting information shows the SEM-EDX of gold films grown at 20 and 40 °C, and a small carbon peak is present for the film grown at 20 °C. Such a carbon peak is what one should expect if the film is contaminated by citrate. For the films grown at 40 and 60 °C (the graph for 60 °C was similar to that of 40 °C; not shown here), no obvious carbon peaks were found. These results suggested that the conductivity of gold film was influenced by the contamination. Such contamination of carbon might not only exist on the surface of gold wires, but also at the coalescence interface (as shown in supporting information Fig. S3). For example, in Fig. 4, small gold nanoparticles coalesce with larger ones, that might lead to trapping of carbon inside the wire.

Previously [17] we observed that the size of the gold films on water surface could be several square centimeters at a growth temperature of 20 °C. While in the current experiments, the area of the gold films at 40 and 60 °C could be as large as the area of the wall that used for deposition, since the films were found covering all the wall area in our experiments. That means, the area of the gold films can be controlled by the surface area of liquid at 20 °C and the area of the wall deposition at 40 and 60 °C. We believe that the method could be extended and used for large area deposition (say a square meter) and then the 20 C method might be most feasible one.

Since the contamination of the films deposited at 40 and 60 °C was almost the same, the two main factors accounting for the difference in conductivity should be the film density and the diameter of the nanowires. From the larger wire diameter in the 60 °C film, one should expect a higher conductivity, which is not the case. Instead, it is the density that is dominating the conductivity properties. The larger density, found by microscopy and transmittance measurement, in the 40 °C films lead to a higher conductivity of these films compared to the 60 °C films.

To demonstrate a simple application of these gold films, we made a hybrid of gold film/gold nanoparticle. The nanoparticles were linked to the film by hexamethylene diamine (HD). Fig. 9(A) shows the TEM image of the hybrid, which shows how the gold nanoparticles are covering the gold wires. The deposition of gold nanoparticles on gold wires increased the diameter of the gold wires, thus, the transmittance should decreased. Fig. 9(B) illustrates the transmittance curves of the original gold film and gold film/gold nanoparticle hybrid. As is shown, the average

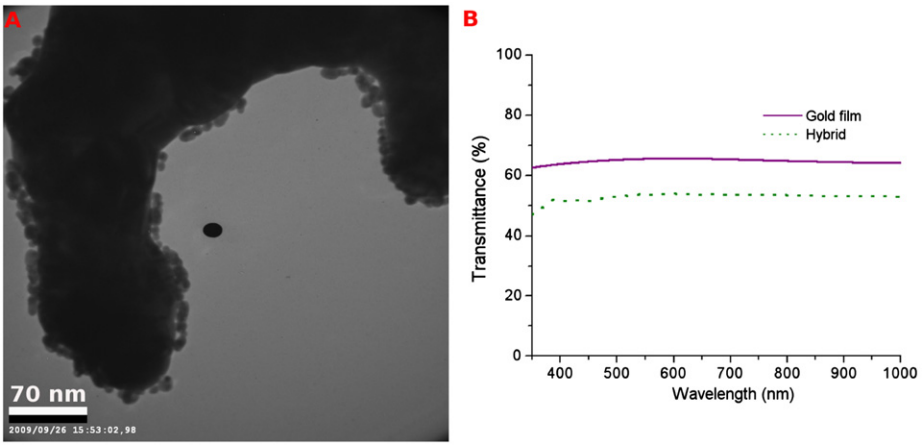


**Fig. 9.** TEM image of gold film/gold nanoparticle hybrid (A) and the transmittance of gold film and gold film/gold nanoparticle hybrid (B).

transmittance decreased by almost 10% after the assembly of gold nanoparticles.

The results suggest that these single layer porous gold films could be used as biosensors, for example, as a DNA hybridization sensor or an immune sensor. Compared with other film deposition techniques that are used for optical biosensors, the gold films here have large surface areas. Moreover, the large surface area is also of importance in, for example, electrochemical determinations, where a large area is needed for low concentration analysis. Also, since the gold film can float on water surface, it is easy to combine electrochemical methods with spectroscopic method simultaneously for characterization of chemical and biomolecules.

## 4. Conclusions

In summary, we investigated the behavior of the growth of porous single layer gold films at different temperature. The densities of these films were highest for the lowest growth temperatures, as revealed by transmittance and electron microscopy. To mimic the growth process, which was hard to observe in the real process, we studied the coalescence of nanoparticles in situ by electron irradiation in a TEM. The in situ TEM measurement showed a linear relationship between time and $(x/r)^6$ as expected. Sheet resistance and I/V measurements showed that films grown at 40 °C had the highest conductivity. The conductivities of the gold films were mainly determined by the level of contaminations in the gold films, the diameters of the gold wires and the densities of the films. The transmittance changes during the hybridization of gold nanoparticles to the gold film suggest potential application of these gold films as sensors.

## Acknowledgements

We thank the Sundsvall Community for financial support. We also thank Mr. Staffan Palovaara for helping with SEM-EDX characterization.

## Appendix A. Supplementary materials

Supplementary data associated with this article can be found in the online version at doi:10.1016/j.physb.2010.08.029.

## References

[1] Y. Luo, J. Ruff, R. Ray, Y.L. Gu, H.J. Ploehn, W.A. Scrivens, Chem. Mater. 17 (2005) 5023.
[2] M. Walther, D.G. Cooke, C. Sherstan, M. Hajar, M.R. Freeman, F.A. Hegmann, Phys. Rev. B 76 (2007) 125408.
[3] H. Lee, E. Kim, H. Yu, J. Jung, W. Chae, Nanotechnolgy 20 (2009) 325604.
[4] F.D. Stefani, K. Vasilev, N. Bocchio, N. Stoyanova, M. Kreiter, Phys. Rev. Lett. 94 (2005) 023005.
[5] F.L. Jia, C.F. Yu, Z.H. Ai, L.Z. Zhang, Chem. Mater. 19 (2007) 3648.
[6] L.H. Qian, X.Q. Yan, T. Fujita, A. Inoue, M.W. Chen, Appl. Phys. Lett. 90 (2007) 153120.
[7] J.T. Zhang, P.P. Liu, H.Y. Ma, Y. Ding, J. Phys. Chem. C 111 (2007) 10382.
[8] S.O. Kuchetev, J.R. Hayes, J. Biener, T. Huser, C.E. Talley, A.V. Hamza, Appl. Phys. Lett. 89 (2006) 053102.
[9] W. Gao, X.H. Xia, J.J. Xu, H.Y. Chen, J. Phys. Chem. C 111 (2007) 12213.
[10] P.N. Bartlett, J.J. Baumberg, P.R. Birkin, M.A. Ghanem, M.C. Netti, Chem. Mater. 14 (2002) 2199.
[11] F.C. Meldrum, R. Seshadri, Chem. Commun. (2000) 29.
[12] L.H. Pei, K. Mori, M. Adachi, Langmuir 20 (2004) 7843.
[13] T. Wang, X.G. Hu, J.L. Wang, S.J. Dong, Talanta 75 (2008) 455.
[14] Y.P. Deng, W. Huang, X. Chen, Z.L. Li, Electrochem. Commun. 10 (2008) 810.
[15] D.D. Brewer, J. Allen, M.R. Miller, J.M. de Santos, S. Kumar, D.J. Norris, M. Tsapatsis, L.E. Scriven, Langmuir 24 (2008) 13683.
[16] D.J. Norris, E.G. Arlinghaus, L.L. Meng, R. Heiny, L.E. Scriven, Adv. Mater. 16 (2004) 1393.
[17] R.Y. Zhang, M. Hummelgård, H. Olin, J. Colloid. Interface Sci. 340 (2009) 58.
[18] J.B. Pang, S.S. Xiong, F. Jaeckel, Z.C. Sun, D. Dunphy, C.J. Brinker, J. Am. Chem. Soc. 130 (2008) 3284.
[19] T. Brezesinski, M. Groenewolt, A. Gibaud, N. Pinna, M. Antonietti, B.M. Smarsly, Adv. Mater. 18 (2006) 2260.
[20] C.J. Brinker, Y.F. Lu, A. Sellinger, H.Y. Fan, Adv. Mater. 11 (1999) 579.
[21] A. Sellinger, P.M. Weiss, A. Nguyen, Y.F. Lu, R.A. Assink, W.L. Gong, C.J. Brinker, Nature 394 (1998) 256.
[22] Y. Chen, R.E. Palmer, J.P. Wilcoxon, Langmuir 22 (2006) 2851.
[23] R.Y. Zhang, X.M. Wang, Chem. Mater. 19 (2007) 976.
[24] N. Kaiser, Appl. Opt. 41 (2002) 3053.
[25] E. Rabani, D.R. Reichman, P.L. Geissler, L.E. Brus, Nature 426 (2003) 271.
[26] R. Werner, M. Wanner, G. Schneider, D. Gerthsen, Phys. Rev. B 72 (2005) 045426.
[27] P. Jensen, A. Barabasi, H. Larralde, S. Havlin, H.E. Stanley, Phys. Rev. B 50 (1994) 15316.
[28] M.Y. Lin, H.M. Lindsay, D.A. Weitz, R.C. Ball, R. Klein, P. Meakin, Nature 339 (1989) 360.
[29] M. Jose-Yacaman, C. Gutierrez-Wing, M. Miki, D.-Q. Yang, K.N. Piyakis, E. Sacher, J. Phys. Chem. B 109 (2005) 9703.
[30] P. Meakin, Phys. Rev. Lett. 51 (1983) 1119.
[31] L.J. Lewis, P. Jensen, N. Combe, J.-L. Barrat, Phys. Rev. B 61 (2000) 16084.
[32] W.S. Coblenz, J.M. Dynys, R.M. Cannon, R.L. Colde, Mater. Res. Bull. 13 (1980) 141.
[33] S. Arcidiacono, N.R. Bieri, D. Poulikakos, C.P. Grigoropoulos, Int. J. Multiphase Flow 30 (2004) 979.
[34] A. Bietsch, B. Michel, Appl. Phys. Lett. 80 (2002) 3346.
[35] S.A. Collette, M.A. Sutton, P. Miney, A.P. Reynolds, X.D. Li, P.E. Colavita, W.A. Scrivens, Y. Luo, T. Sudarshan, P. Muzykov, M.L. Myrick, Nanotechnology 15 (2004) 1812.